The Ocean Osmotic Engine Philip L. Brewbaker (midbrew@yahoo.com) 8/14/2024

In 2008 the Norwegian company Statkraft tested an Osmotic Engine using Reverse Osmosis (RO) membranes [1-3]. The engine is designed to introduce fresh water to ocean water in such a way as to tap into the chemical potential energy of their relative salinity and turn that into electricity. A schematic of the engine is shown in Figure 1.

Figure 1: Osmotic Engine Schematic

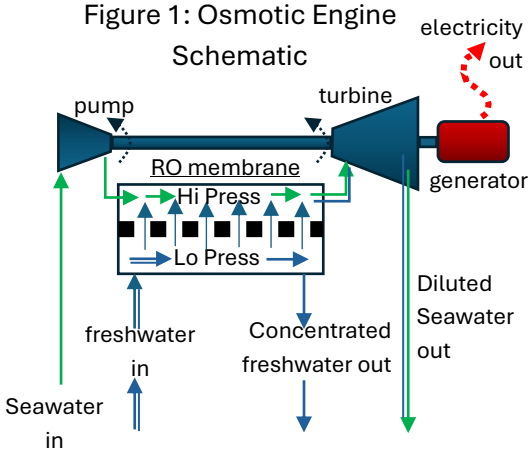

Seawater pumped from the ocean is first pressurized to about 200psig. It is then introduced to the permeate side of an RO module, and fresh water, at atmospheric pressure, is introduced to the feed side. Against the pressure gradient the fresh water crosses the RO membrane, drawn in by the salt in the seawater. The seawater swelled with fresh water is then passed through a turbine to generate electricity and discharged back into the ocean. This process draws electricity from fresh water which typically would enter the ocean anyway and lose that energy as heat. The cost of power from an Osmotic Engine could be competitive with other forms of energy, such as wind or solar [4, 5].

The ocean osmotic engine discussed here moves the osmotic engine 400 ft deep into the ocean, where seawater is already at 200 psi, where the necessary seawater for the power plant is abundant and where coastal conflicts are less of a factor. Figure 2 shows the basic schematic of this ocean-based osmotic engine. Incoming freshwater is pre-treated, channeled through a feedpipe down to the engine. It enters the water turbines at 200psi and leaves at 0psi. The turbines transmit their mechanical energy to the generator, where it is turned into electricity, and channeled back to shore. Meanwhile, the freshwater that leaves the turbines at 0psi enters the RO exchangers, where its affinity for salt draws it out into the ocean despite the 200psi pressure gradient it must climb to get there.

Figure 2: Ocean Osmotic Engine Schematic

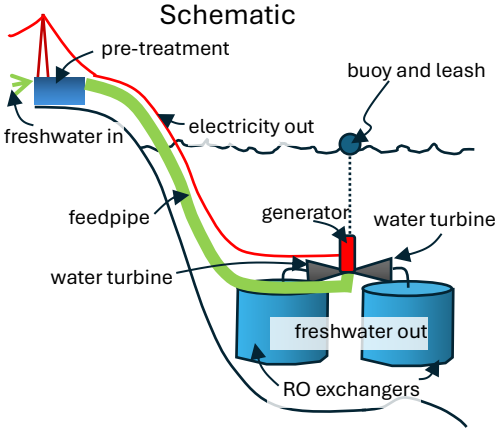

To balance the forces on the power plant, two water turbines are needed, each pulling in opposite directions as the freshwater is depressurized. The depressurized feedwater is channeled into two or more RO exchangers. Nominally, these are configured as spiral wound modules. These RO exchangers are about 100 feet in diameter and 25 feet tall. The ability of the ocean to easily accommodate the large RO membrane area required in this application is an important factor in placing it in the ocean.

Figure 3 shows the appearance of a single Ocean RO power plant from a CAD model.

Figure 3: A single ocean RO power plant: CAD drawing

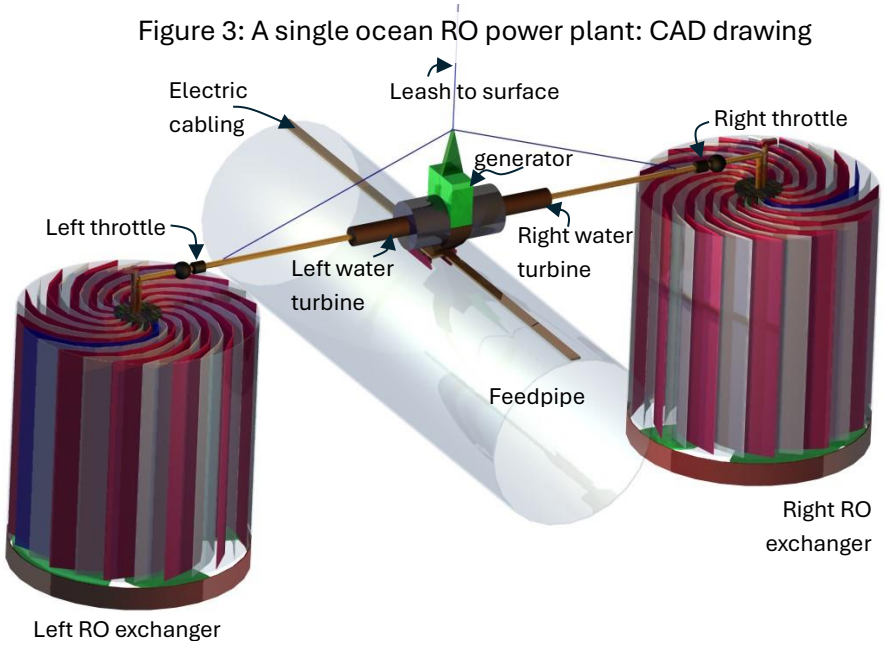

Each modular power plant would be held vertically in the ocean by a leash attached to a buoy. The weight of the power plant would be mostly offset by attached buoyancy, so that the surface buoy is used primarily to ensure proper depth placement rather than to carry the entire weight of the power plant itself.

The advantage of an ocean-based power plant is that the ocean doesn't need to be piped up to the power plant. The disadvantage is that the freshwater needs to be piped to the ocean. Note that the freshwater feedpipe does not need significant structural hardening, as at each point in its journey, the freshwater inside it is at the same pressure as the seawater outside. That is, the pipes' primary purpose is as a chemical barrier, not a mechanical or thermal one. Made of low-density polyethylene (LDPE), about 15mil thick, or another plastic with a density approximately that of water and glued to fish netting for tear resistance, and mounted on buoys every half-mile or so, the feedpipe can serve as an inexpensive conveyance. In Figure 3, it is pictured as having a large diameter to reduce kinetic forces as it conveys freshwater to the sunken power plant.

Figure 4 shows a schematic of the parts of a single Ocean RO power plant. The power plant is designed so that as freshwater flows in, it splits into two flows travelling in opposite directions. Each flow encounters a helical water turbine, and each turbine pulls on the other. Their mutual repulsion is balanced by their mechanical connection, so that the net force on the power plant is zero. Looking outward along the axis of the turbine, toward the low-pressure end, each turbine would be designed to turn clockwise. In this way, their angular momentums cancel. At the low-pressure end of each turbine is a remotely operable throttle valve. Software would be in control of each valve to fine-tune the forces on the turbine assembly, so that they cancel. Note that these valves are also necessary during maintenance and repair to shut down the power plant. For

example, if a leak develops in either RO exchanger unit, both valves would have to be shut, and the entire unit raised for repair. Given the criticality of the valve function, it may be necessary to back up each valve with a gate valve, to ensure each power plant can be shut down with 100% reliability.

Figure 4: Schematic for an individual 2 MW ocean RO power plant

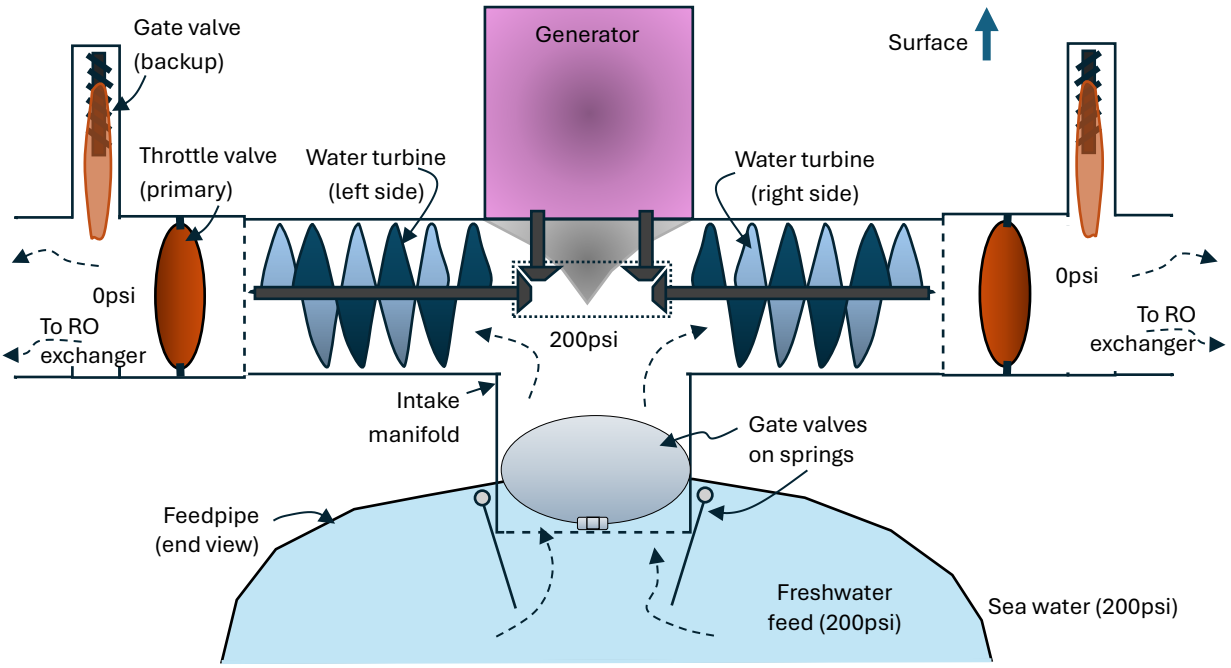

Because the freshwater in the feedpipe is at the same pressure as the seawater outside it, the gate valves that must open when the power plant is attached to it don't require extra hardening against pressure and can be spring-loaded. This is indicated in Figure 4. As the power plant is lowered onto the feed pipe, it pushes two doors downward into the feedpipe. Then, when the throttles are opened for freshwater to flow into the power plant, the drop in pressure opens a similar spring-loaded trap door inside the power plants intake manifold. These simple mechanisms ensure 100% reliability while serving adequately to keep freshwater and seawater from mixing when the power plant is raised for maintenance. While freshwater is flowing between the feedpipe and the power plant, its pressure is just below that of the surrounding seawater, which helps press them together without further mechanical means and maintains the water seal between them.

Automatically-actuated or remotely-actuated valves are important in this application so that each power plant can be raised and lowered as needed to the surface for maintenance and part replacement. The goal is to make maintenance as inexpensive as possible given the deep ocean environment.

This concept extends to the electrical power line that comes off the generator and plugs into the power line that runs along the top edge of the feedpipe. Refer to Figure 5, which shows the power plant positioned 10 feet above the feedpipe.

Figure 5: Power plant/feedpipe connections

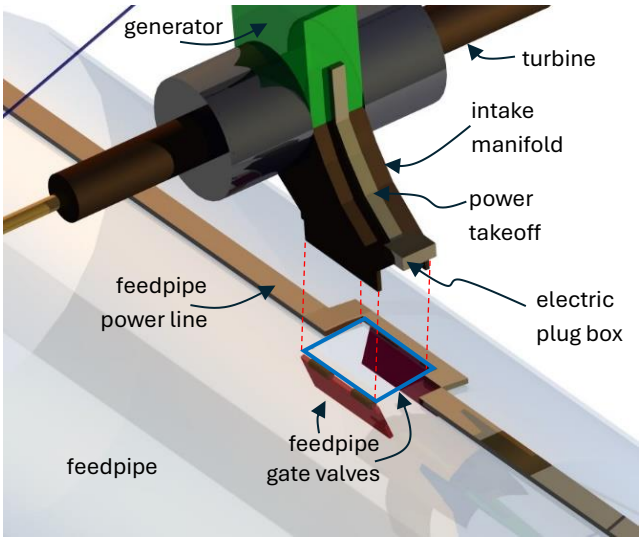

The electrical plugs that connect the generator power takeoff line to the matching plugs on the feedpipe would need a special design. They would need a method of mechanical guiding, so as the power plant is lowered, the plugs align. They would also need corrosion protection, so that when unplugged they are isolated from the corrosive seawater. One such design is indicated in Figure 6. The two halves of an electrical plug are surrounded by deionized freshwater when in an unplugged condition. When plugged together, the freshwater is held in nearby bellows. The bellows are designed so that at any depth, the water inside the plug is at the same pressure as the seawater outside it, which reduces the likelihood of leakage past the rubber seals. These are preliminary designs.

Figure 6: Low-corrosion-rate electric plugs

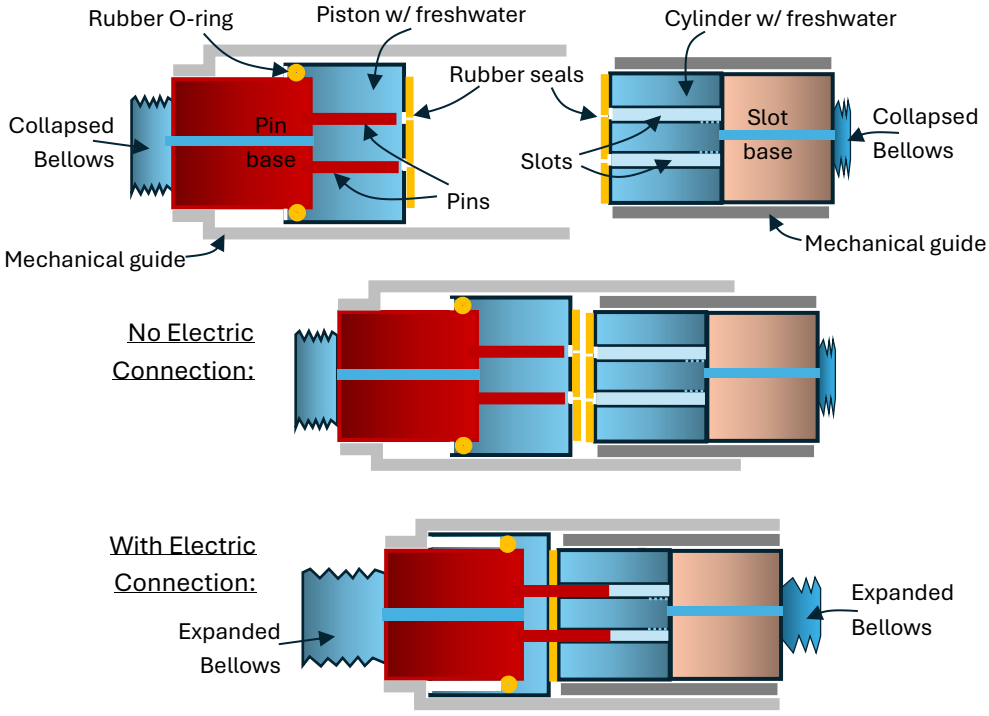

The feedpipe could conceivably be designed to issue freshwater to more than one power plant, as shown in Figure 7. The feedpipe could branch as needed to allow individual power plants to string along it, following the coastline.

Figure 7: Schematic for a 14 MW ocean RO power facility

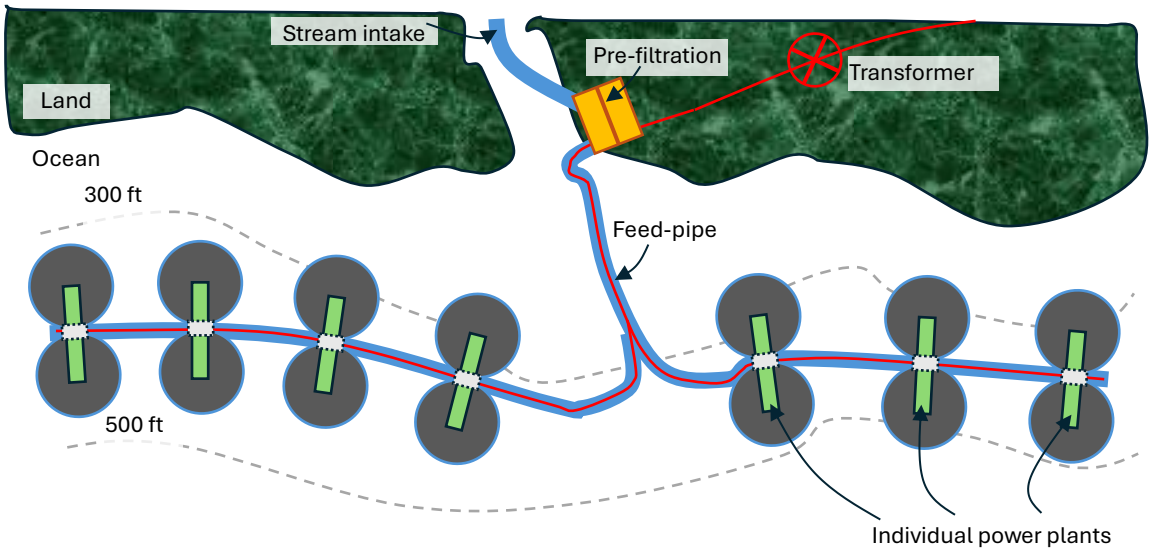

By setting up the feedpipe beforehand to accommodate a flexible number of power plants strung along it, individual power plants can be raised and lowered without interrupting the others. In maintenance, then, an individual power plant would be raised up to the maintenance vessel.

The RO exchangers are nominally designed as spiral-wound modules. Unlike land-based spiral modules, they are loosely packed and, although surrounded by a sleeve of flexible polyethylene, are not packed tightly within a pressure vessel. A 2MW power plant requires two RO exchangers. Each RO exchanger totals about 210,000 m^2 of membrane area. Assuming 20 leaves of spiral wound material and a 2" gap between leaves, the module would be about 25 feet tall and 100 feet in diameter. Each leaf is composed of two RO membranes surrounding a feed spacer, as shown in Figure 8. The feed spacer is 33mil thick, as in a normal spiral wound RO module. Note that the same membrane area can be obtained from a variety of combinations of height, diameter, leaf gap, and number of spiral wound units, which could be stacked vertically. The goal is membrane area, not a particular configuration for achieving that area. Even the spiral-wound geometry is negotiable.

Each spiral wound RO exchanger, or vertically stacked system of RO exchangers, is under-girded by a seawater pump, which resembles a large fan with the same diameter as the spiral wound module. Although the pump is large, the pressures developed by it are very small since frictional losses on the permeate-side of the leaves of the exchanger are very small, hence it robs very little of the power from the power plant. It is designed to push seawater past the exchanger to replace seawater in the exchanger that has been diluted by freshwater. Diluted seawater has a lower density than undiluted seawater so buoyancy will pull it upward. The seawater pump aids in that

flow direction. It also pulls the RO exchanger gently downward against the surface buoy, thus keeping the tether taut, and helping to maintain the connection between the power plant and the feedpipe.

Figure 8: Schematic of freshwater flow in the leaves of an RO exchanger

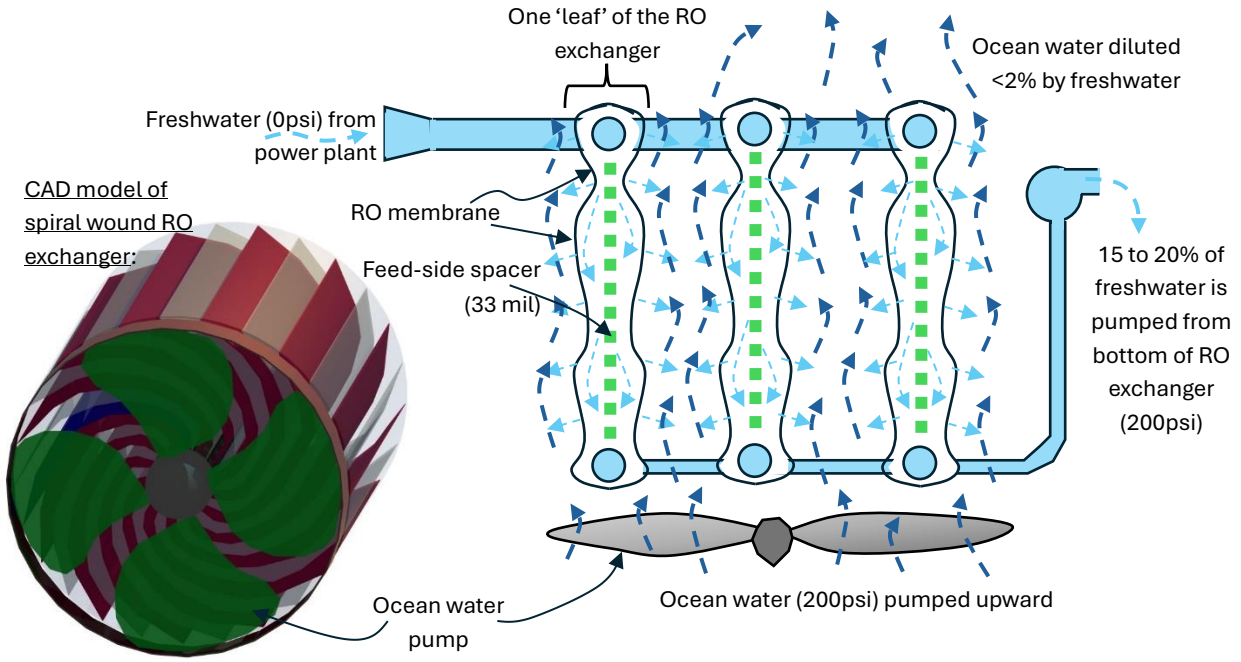

A larger source of lost power comes from the freshwater that exits the RO exchanger. This exiting freshwater comprises about 15% to 20% of the incoming freshwater. To be dumped to the ocean it must first be pressurized to the ocean's pressure, which can cost 20-30% of the output power from the turbine. Although the power plant can be optimized to reduce this parasitic loss, it can't be eliminated. Therefore, the output to the feed side of the RO exchanger must lead to a pump, as shown in Figure 8.

Maintenance and Replacement

In maintenance, the entire power plant would be raised on its tether to the surface (due to attached buoyancy, the power plant needn't be overly heavy). At the surface, the turbine and generator sections would be isolated from the RO exchanger sections, hauled aboard the vessel, and worked on there.

The RO exchanger sections, due to their size, would ideally be maintained while in the ocean. Note that in a normal RO process both the salt and the water are travelling in the same direction, from the feed side of the membrane to the permeate side. This exacerbates membrane fouling, as minerals and contaminants entrained by the water get left behind at the membrane surface. However, in this application salt is traveling in the opposite direction as water. Driven by the concentration gradient from the seawater to the freshwater side, salt is going in one direction.

Driven by the Osmotic pressure gradient, water is going in the other direction. It is felt that this would retard membrane fouling because the motion of the water solvent will help sweep salt away from the membrane on the seawater side where salt is the greater threat to fouling.

Figure 9 shows a proposed method to clean the RO exchangers while they remain in the ocean. It would be necessary to lower a cap to go over the permeate (seawater) pump at the bottom of the exchanger. This cap would be connected to a vertical pipe to the surface, such that when the permeate pump is actuated, it pumps seawater out of the permeate-side of the RO exchanger, replacing it with cleaning fluid. Once the seawater is removed, the cleaning fluid can be recirculated by the permeate pump to clean the RO membrane surface, on the outside. Simultaneously, on the inside, cleaning fluid would be circulated by the feed exit pump in a closed loop.

Figure 9: Cleaning the RO membrane in the ocean

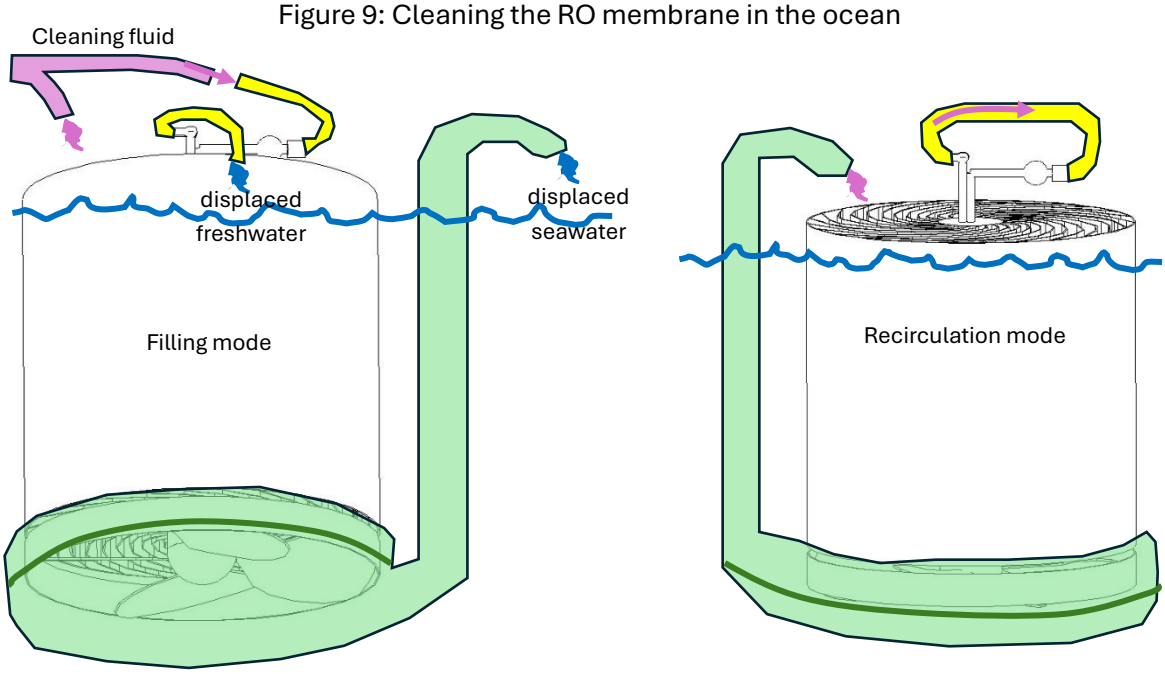

The RO exchangers will likely be towed to and from the site, due to size and their compatibility with the ocean environment. Note that an exchanger 100 feet in diameter with a 2 inch permeate-side gap between the leaves can be compressed to 53 feet in diameter if the gap is tightened for transport to ½ inch.

Design considerations

An economic analysis of the Ocean RO power plant has yet to be performed. A major cost factor will be the cost of the membranes themselves. Maintenance will also be a higher cost item than a land-based plant, although careful design choices may ameliorate this factor somewhat. Below 400 ft, the power plant is in still, cold, deoxygenated water: the major issues are corrosion protection and ease of attachment/detachment for maintenance at the surface. Depending on the site, other issues could be deep water ocean currents and ocean life, such as marine mammals.

The uniqueness of this application requires a novel design for the RO exchangers. A spreadsheet was set up to help with this. Table 1 shows typical input and output for this spreadsheet.

The membrane-specific parameters input to the design are the water permeability 'A' (m/s-Pa) and salt permeability 'B' (m/s). Appendix A discusses how these parameters are derived.

Geometry-specific parameters are items specific to a spiral-wound module, like diameter, height, number of leaves, and leaf gap. Note that while the permeate (seawater) side leaf gap is flexible, the feed (freshwater) side leaf gap should be chosen to be consistent with feed spacers used in standard RO spiral wound modules. Otherwise, the concentration polarization equations developed for those feed-side standard spiral wound geometries won't work properly for this application (see Appendix B). A standard 33mil feed side spacer is currently assumed.

Table 1: RO exchanger design spreadsheet - example

				Design Characteristics:								23%				Props of Water:					
RO spiral wound exchanger:					Total	Core	Exchanger Location:					RO Membrane:					Cp	4190	J/kg-K		
Exchngr height (ft)	22.7			Width/leaf (ft)	2291	0.9	Depth of top (ft)	430	131 m				Make:	Model:			Temp:	4	20		
Exchngr Diam (ft)	100.0			Net W/leaf (ft)	2290		Pressure (psi)	191					FilmTec:	XLE-440		rho (kg/m3):	1026	1024	for S=34 ppt		
Core Diam (ft)	2.0	dh (m)		W*H/leaf	4832	m2	kPa	1318	13 bar			At Manuf(25C)		At this use T:		mu (N-s/m2)	0.001537	0.00102			
Feed gap (in)	0.033	0.00168		Total W*H	96637	m2	Ocean condition at this depth:		T			A (m/s-Pa):	2.18E-11	1.66E-11		nu (m2/s)	1.50E-06	9.95E-07			
Permeate gap (in)	2.0	0.10160		ExchangeArea	193273	m2	Cp (ppm)	34000	16 C			B (m/s):	1.12E-07	8.55E-08		Pr	11.24	7.09			
RO membranes+extra(in)	0.024			Fluid X-sec area:			density (kg/m3)	mu (N-s/m2	nu (m2/s)	D (m2/s)	Sc					k (W/m-K)	0.578	0.602			
Spacing (in)	2.06			feed (m2)	11.7		1025	0.00115	1.13E-06	1.41E-09	796					D salt in water (m2/s):	1.31E-09	1.45E-09	m2/s		
# leaves:	20			permeate (m2)	709			OsmP/Conc	72	Pa/ppm						Sc:	1140	686			
Space/leaf (in)	41				for Del P	for Sh															
Spiral 'a' value (in)	6.55			Shrivathsan X:	0.297	0.65															
#windings	14.6																				
																		Net			
Five Node Mini-Model to estimate Cf avg:					Cf avg:	2189						Output (node10):		Qout gpm	Cout ppm	rec	Power kW		ratio of rec		
	Node 1	Node 2	Node 3	Node 4	Node 5		Ten Node Model:					feed		3853	4906	79%	1224	one/ten	100%		
Cf (ppm)	700	995	1486	2333	3577							permeate		2839826	33821	Cf in node€	1641	five/ten	97%		
Cfavg/Cf in:	1.20	1.21	1.25	1.29	1.27	1.12	Node 1	Feed side calcs:				Permeate side calcs:				Salt calcs:	Feed		ppm		
Qsalt (kg/s)	0.0792	0.0777	0.0749	0.0700	0.0634			β f guess	1.38			β p guess	0.722				Cin (kg/m3)	0.7	700		
Salt out (kg/s)	0.8983	0.9760	1.0508	1.1208	1.1842		1.106		J (m/s)	6.32E-06							Salt in (kg/s)	8.19E-01			
Qthru (m3/s)	2.68E-01	2.46E-01	2.06E-01	1.37E-01	4.44E-02	rec			Jsalt(ppm*m/s)	2.01E-03							Salt out (kg/s)	8.58E-01	ppm		
Qout f (m3/s)	9.02E-01	6.57E-01	4.50E-01	3.13E-01	2.69E-01	77%			Qthru (m3/s)	1.22E-01	1947	gpm					Cout (kg/m3)	0.82	819		
Cout (ppm)	995	1486	2333	3577	4403		gpm		Qsalt (kg/s)	0.0388				gpm			Cf avg/Cf in	1.085			
							18645		Qin f:	1.17E+00	<-m3/s->	Qin p:	177.29	2825033			Permeate		ppm		
One Node Model:						kW	16698		Qout f:	1.05E+00	<-m3/s->	Qout p:	177.41	2826980			Cin (kg/m3)	34	34000		
β f guess	1.30	-0.1%			Power out:	1543			v f (m/s)	0.100		v p (m/s)	0.25				Salt in (kg/s)	6027.8			
β p guess	0.7375	0.2%		Permeate pump loss:		28			Re f	149		Re p	22574	f guess:			Salt out (kg/s)	6027.8	ppm		
J (m/s)	4.83E-06			Concentrate pump loss:		313			f Schock&Miguel	3.1		f:	0.071	0.072			Cout (kg/m3)	34.0	33976		
Jsalt(ppm*m/s)	1.90E-03				Net Power:	1202			P loss (psi)	1.0		P loss (psi)	0.002	2.8	<- f multpl						
	In	Thru	Out	rec		78%	Sh: Shriva	Chen&Quir	Qui&Davies			Sh nonporous2	788								
feed (m3/s)	1.17E+00	9.33E-01	2.37E-01	80%			186	33	7			Sh nonporous	1487								
gpm	18645	14863	3782				Sv:	Use Sh:	Chen&Quin			Sh porous	1409								
Salt (kg/s)	0.8191	0.3673	1.1864				32	k (m/s)	2.75E-05			k (m/s)	1.96E-05								
C (ppm):	700	2181	4998					β feed approx	1.258			β feed approx	0.724								
Feed side calcs:			Permeate side calcs:																		
v f (m/s)	0.10		v p (m/s)	0.25				β feed	1.375			β feed	0.722								
Re f	149		Qin p (m3/s)	177.29	2825033	gpm		% diff β f	-0.1%			% diff β f	0.0%								
f Shrivathsan	6.0		Qout p (m3/s)	178.22	2839896	gpm	Node 2	Feed side calcs:				Permeate side calcs:				Salt calcs:	Feed		ppm		
f Schock&Miguel	3.1		Re p	22574	e/dh:			β f guess	1.38			β p guess	0.721				Cin (kg/m3)	0.819	819		
P loss (psi)	10		Roughness e (m):	0.005	0.0492				J (m/s)	6.06E-06							Salt in (kg/s)	8.58E-01			
Sh lam	13		f guess:	0.072	f multpl:				Jsalt(ppm*m/s)	1.99E-03							Salt out (kg/s)	8.96E-01	ppm		
Sh turb	12		f:	0.071	2.8				Qthru (m3/s)	1.17E-01	1868	gpm					Cout (kg/m3)	0.96	963		
Sh Shrivathsan	186		P loss (psi)	0.023			gpm		Qsalt (kg/s)	0.0384				gpm			Cf avg/Cf in	1.088			
Sh Schock&Miguel	33		ratio of δ values:	1.28			16698		Qin f:	1.05E+00	<-m3/s->	Qin p:	177.41	2826980			Permeate		ppm		
Sh Chen&Quin	33		Sh from β guess	1139			14831		Qout f:	9.31E-01	<-m3/s->	Qout p:	177.53	2828848			Cin (kg/m3)	34.0	33976		
Sh Qui&Davies	3		Sh nonporous2	788					v f (m/s)	0.090		v p (m/s)	0.25				Salt in (kg/s)	6027.8			
Sv:	25		Sh nonporous	1487					Re f	133		Re p	22589	f guess:			Salt out (kg/s)	6027.8	ppm		
Sh correl to use:	Chen&Quin		Sh porous	1162					f Schock&Miguel	3.3		f:	0.071	0.072			Cout (kg/m3)	34.0	33954		
k (m/s)	2.75E-05		k (m/s)	1.62E-05					P loss (psi)	0.8		P loss (psi)	0.002	2.8	<- f multpl						
β feed approx	1.192		β feed approx	0.742					Sh: Shriva	Chen&Quir	Qui&Davies		Sh nonporous2	788								
β feed	1.299		β feed	0.739					173	29	7		Sh nonporous	1488								
% diff β f	-0.1%		% diff β p	0.2%					Sv:	Use Sh:	Chen&Quin		Sh porous	1339								
									29	k (m/s)	2.49E-05		k (m/s)	1.86E-05								
										β feed approx	1.276		β feed approx	0.722								
										β feed	1.387		β feed	0.720								
			time to mid: tm (s)		14					% diff β f	0.2%		% diff β f	-0.2%								

Both feed- and permeate- side fluids are assumed to pass by the membrane surface in one sweep, from top to bottom (the permeate-side seawater may go from bottom to top). As the feed side freshwater does this, its salt content builds up due to loss of water and salt diffusion across the membrane from the seawater. In Table 1, it enters at 700ppm salt content and exits at 4900ppm.

The depth of the RO exchanger is input as it governs the mechanical pressure gradient across the membrane. The salt content of the freshwater and the seawater are input since they determine the osmotic pressure (OsmP) across the membrane.

The equations that govern how these membrane parameters and geometry parameters interact are discussed in Appendix A. In the spreadsheet, two models are maintained, a one-node model and a ten-node model (the one-node model is supported by a five-node mini-model to aid in salt-balancing). Only the first two nodes of the ten-node model are shown in Table 1. The two models serve as a check on one another. The ten-node model is more accurate, but the difference in output power is less than 1%.

The spreadsheet was used to examine several performance factors helpful in choosing the optimum RO exchanger. In Table 1, the output is for a 23 ft high, 100 ft diameter spiral wound module of 20 leaves, using a brackish-water-specific RO membrane (BWRO), at a depth of 430 ft, in which the feed-side water velocity is 10 cm/s and the permeate-side water velocity is 25 cm/s.

One way to reduce the amount of membrane required in this application is to reduce the concentration polarization boundary layers that build up on either surface of the membrane. Increasing the Reynolds Number will reduce this layer. The primary way, for a fixed geometry, is to increase the velocity, although too large an increase will significantly impact the net power from the system. The feed-side (10 cm/s) and permeate-side (25 cm/s) water velocities shown in Table 1 were selected this way, although the search effort wasn't exhaustive. The effect of feed-side velocity is discussed below (see Figure 12). Appendix B discusses the optimization of the permeate-side water velocity.

Another way to increase the Reynolds number is through surface roughness. This was not examined in any detail. This offers limited attractiveness on the feed-side, as it is already so narrow (33 mil) and crammed with the feed-side spacer. On the permeate-side, Table 1 currently assumes that some fish-netting has been glued to the membrane there, to improve its roughness, but this is only preliminary, and in the future more should be done to induce turbulence on that side of the membrane.

Another way to reduce the cost of the RO exchangers is to specify inexpensive membranes. Such membranes would likely be marginal in a normal RO operation where the objective is to produce high quality freshwater from brackish or seawater. Here the objective is to maximize water transport while maintaining a reasonable osmotic pressure gradient.

In Table 2 and Figure 10, three different FilmTec membranes [15] are examined for this application. Each is designed to produce 1.2 MW of net power from one-half of an Ocean Osmotic Power Plant (i.e. from one turbine and one RO exchanger).

Table 2: Three FilmTec membrane materials [15] (permeabilities are given as the ratio with those of the seawater membrane: SW30XLE-400i)				
Membrane	Water Permeability Ratio* (A/A_{sw})	Salt Permeability Ratio*(B/B_{sw})	Net Power (kW)	Membrane Area (m^2)
SW30XLE-400i	1	1	1206	493,800
BW30-400-FR	2.4	1.8	1202	272,400
XLE-440	5.8	4.0	1202	193,300
*for SW30XLE-400i: A_{sw} = 3.76E-12 m/s-Pa (0.055 GFD/psi), B_{sw} = 2.83E-8 m/s (0.06 GFD)				

The seawater RO membrane material (SW30XLE-400i) requires over twice as much area as the two brackish water materials. Of the two brackish water membranes, one (BW30-400-FR) has higher fouling resistance and better cleanability [15], while the other (XLE-440) has twice the water permeability of the other, but as Figure 10 shows, its impact on reducing the required exchanger area is relatively small. The XLE-440 material, if found to be acceptable for this application, would require further optimization of the concentration polarization layers to determine the optimum design. The XLE-440 results are the ones shown in Table 1.

Figure 10:

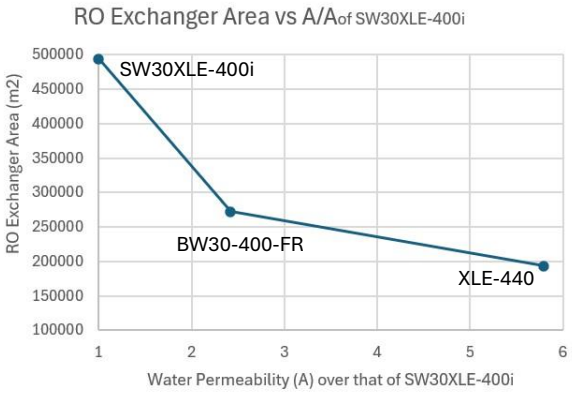

It appears that the increased salt permeability of the brackish water membranes is less significant, in this application, than the increased water permeability.

Two other design parameters examined via the RO exchanger spreadsheet were the effects of depth in the ocean, and of feed-side (freshwater) velocity. In Table 1, the Osmotic pressure, OsmP, given the salt contents of the two inputs, is 350psi, since OsmP = 72Pa/ppm*(34000ppm -700ppm). The maximum power density expected from an Osmotic Engine is generally expected to occur when P = 0.5*OsmP [4]. In this case that is 175psi, so the depth of operation in Table 1, which generates 191psi of pressure, may be a little deep for the optimum.

Figure 11 shows results for a BWRO membrane run at various depths, assuming incoming freshwater at 700ppm salt content, and seawater at 34,000ppm. The overall size of the exchanger is held constant as depth is changed. In particular, the same exchanger height means that at 500 ft depth, there is only a 66% recovery of permeate from feed, whereas at 400 ft it's 86%. Basically, the exchanger is undersized for the 500 ft depth. In an eventual economic analysis, such trade-offs, of depth and size, should be examined to determine the optimum design.

Figure 11: Effect of Depth (ft) on Net Power (kW)

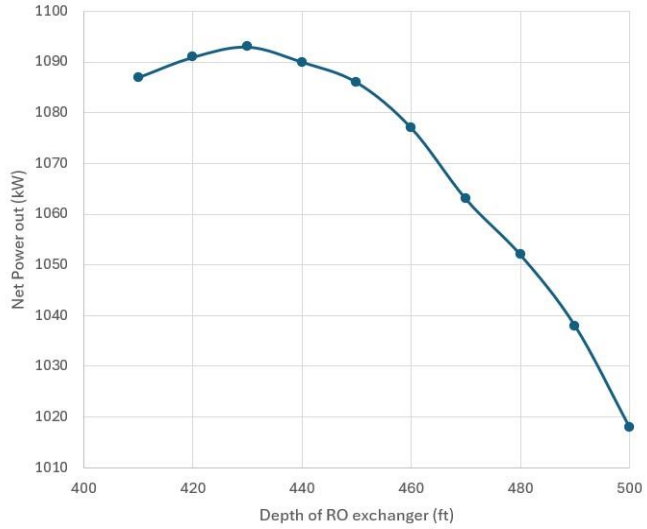

In Figure 12, the effect of feed velocity was examined. In this BWRO-membrane analysis the depth was held constant at 430 ft, but the exchanger height was increased as needed to maximize the net power (keeping the diameter constant at 120 ft). A higher feed velocity is optimized with a longer exchanger. This is why a 3 cm/s feed velocity produces one-third as much power as a 12 cm/s feed velocity. When the power is normalized (to the area optimized for the 6 cm/s feed velocity) feed velocity drops out as a factor. The RO membrane material cost should be proportional to area, but since it is not the only cost in the system, the larger RO exchanger will likely produce cheaper power overall. These are the kinds of trades possible in an economic analysis that uses the RO exchanger spreadsheet. For example, it may be useful in the future to look at turbulence enhancement on the permeate side of the membrane to help break down the concentration boundary layer there, and further optimize net power out per RO membrane area.

Future economic analysis would have as its goal the optimization of the various parts of the Ocean RO power plant, so power can be offered at competitive prices. Part of this will be to find ways to reduce what is expected to be the high maintenance costs of this system, and part to explore how economies-of-scale might be used to reduce capital costs.

Figure 12: Effect of feed velocity on Net Power

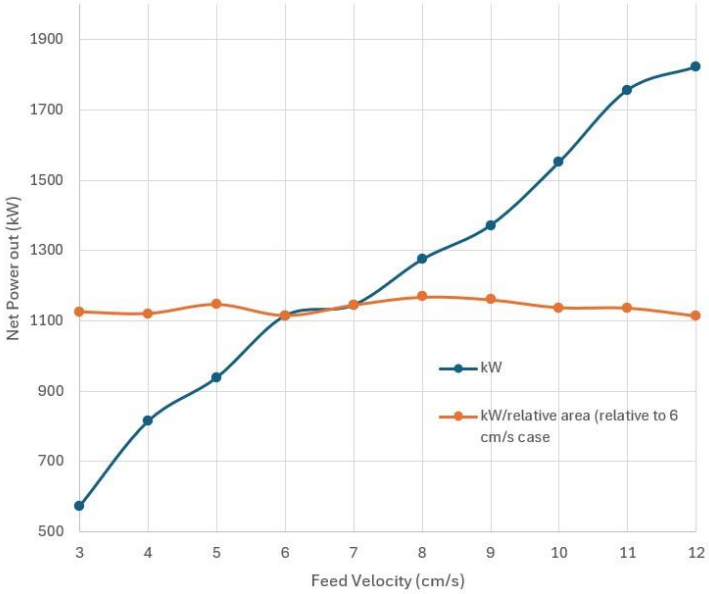

Figure 13: Cost of electricity versus overall system permeability [4]

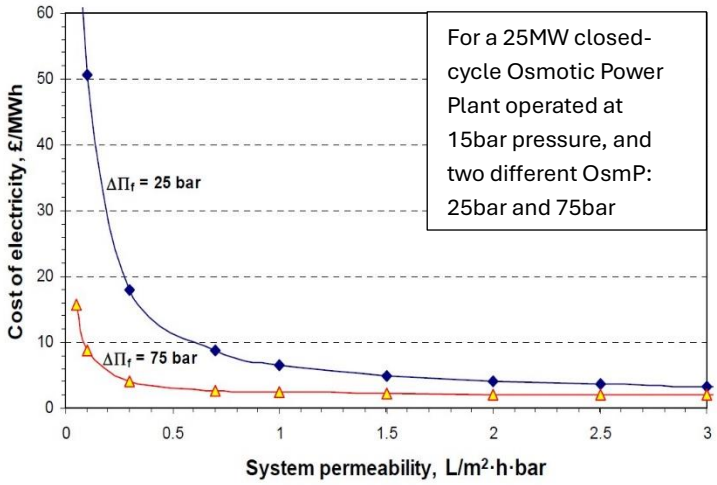

Sharrif et al [4] calculated that a 25MW land-based closed-cycle Osmotic Power Plant, operated at a pressure of 217psi (i.e. similar to the pressure used in Table 1) should have a levelized cost of electricity (in 2014 British pounds/MWh) that is a function of overall system permeability as shown in Figure 13. In Figure 13, the 25bar line is of interest since that is the OsmP of freshwater over seawater. In the example given in Table 1, the overall membrane system permeability was calculated to be 1.78 L/m2-h-bar (it is a function of the membrane permeability and the operating conditions). Hence, according to Figure 13, to be cost competitive the Ocean RO system would aim to provide power at 5 £/MWh, or 8 $/MWh, given the exchange rate in 2014.

References

1. Statkraft Osmotic Power Plant. Power Technology, Oct 29, 2009.

2. Statkraft Osmotic Power Prototype in Hurum. Wikipedia, April 1, 2023.

3. Statkraft Halts Osmotic Power Investments. Statkraft website, Dec 20, 2013.

4. Theoretical and Experimental Investigations of the Potential of Osmotic Energy for Power Production. Sharif, Adel O., Merdaw, Ali A., Aryafar, Maryam, and Peter Nicoll. Membranes 2014, 4, 447-468. ISSN 2077-0375.

5. Osmotic Power. Alex Myers. Holland College. Word Press.

6. Fundamentals of Heat and Mass Transfer, 6th Edition. Incropera, Frank P., DeWitt, David P., Bergman, Theodore L., Lavine, Adrienne S. © 2007, John Wiley & Sons.

7. Seawater Reverse Osmosis Desalination: Assessment and Pre-treatment of fouling and scaling. Salinas-Rodriguez, Sergio G., Schippers, Jan C., Amy, Gary L., Kim, In S., Kennedy, Maria D. May 2021. IWA Publishing.

8. Modeling of Fluid Flow in Spiral Wound Reverse Osmosis Membranes. Srivathsan G. July 2013. University of Minnesota Twin Cities. Dr. Ephraim Sparrow. Retrieved from the University Digital Conservancy, https://hdl.handle.net/11299/158160.

9. Concentration polarization model of spiral-wound membrane modules with application to batch-mode RO desalination of brackish water. Qiu, T.Y., Davies, P.A. July 15 2015. Sustainable Environment Research Group, School of Engineering and Applied Science, Aston University, Birmingham, B4 7ET, UK. Also from Desalination Vol 368(p 36-47).

10. A Mathematical Modeling of the Reverse Osmosis Concentration Process of a Glucose Solution. Chenghan Chen and Han Qin. 8 May 2019. MDPI Processes 2019, 7(5), 271; https://doi.org/10.3390/pr7050271.

11. Mass Transfer and pressure loss in spiral wound modules. G. Schock, A. Miquel. Desalination, 64 (1987) 339-352.

12. Munson, Young& Okiishi's Fundamentals of Fluid Mechanics 8th Edition. Gerhart, Andrew L., Hockstein, John I., Gerhart, Philip M. Dec 2018. John Wiley&Sons.

13. Design Advantages for SWRO using Advanced Membrane Technology. Bartels, Dr Craig R, Franks, Rich, and Bates, Wayne. 2007. Hydranautics, A Nitto Denko Corporation.

14. Effect of New Generation of Low Pressure, High Salt Rejection Membranes on Power Consumption of RO Systems. Wilf, Dr Mark. 2000. Hydranautics, A Nitto Denko Corporation.

15. FILMTEC™ Membranes: Product Information Catalog. LennTech Water Treatment Solutions © 1998-2024.

16. DuPont FilmTech[tm] Reverse Osmosis Membranes Technical Manual. Feb, 2023. DuPont. Form No. 45-D01504-en, Rev. 16

Appendix A: Modelling the Osmosis Process for the Ocean RO Engine

The water treatment industry has commonly used parameters to define RO membrane systems. The uniqueness of this application required an understanding of two more fundamental parameters, the water permeability, A, and the salt permeability, B. Both are tied uniquely to the membrane itself and not to the water-filtering system it is a part of.

Water flows across the membrane in proportion to the pressure difference across it. The constant of proportionality is A, the water permeability. The resistance to flow is primarily hydraulic, as if the water is being mechanically pushed through very small pores. The pressure is not just mechanical pressure but osmotic pressure as well.

The equation defining the water permeability is:

$$J = A*(P - OsmP) \quad (A1)$$

Where J = water flux across the membrane per area (GFD (gallons/ft^2-day), or m^3/s-m^2)

A = water permeability (m/s-Pa or GFD/psi)

P = mechanical pressure difference across the membrane (Pa or psi). In this application the permeate, seawater, is pressurized to about 200psig, while the feed side is at 0psig.

OsmP = osmotic pressure difference across the membrane (Pa or psi)

Osmotic pressure, the mechanical expression of the affinity salt has with water, can be calculated from the salt concentration as:

$$OsmP = iRT*(C_{mp} - C_{mf}) \quad (A2)$$

Where i = van't Hoff index = 2 for NaCl since it dissolves into 2 ions. They don't dissolve ideally and there are other ions in seawater, so a better value is 88% of 2.

R = ideal gas constant = 8314 J/kmole-K. Note that iR = 2*0.88*8314 J/kmole$_{salt}$-K. This can be divided by 58.44 kg/kmole (seawater is mostly NaCl and this is its MW) to get units of J/kg$_{salt}$-K or N-m/kg$_{salt}$-K. Multiply this by (1 kg$_{salt}$/m$^3_{solution}$/1000 ppm), to get units of N-m/m$^3_{solution}$ -ppm = Pa/ppm. That is iR = 2*0.88*8314 J/kmol$_{salt}$-K = 0.2504 Pa/ppm-K.

T = absolute temperature (K). For room temperature seawater (25 C), iRT = 75 Pa/ppm. In Table 1, where the RO membrane is at 16C, iRT = 72 Pa/ppm. Note that 6894.7 Pa = 1psi.

C_{mp} = salt concentration, C, on membrane surface, m, permeate side, p, (ppm). In this application, the permeate side of the membrane has ordinary seawater circulating past it, at 34000ppm. Because it is at the membrane surface rather than in the bulk flow, C_{mp} is slightly different from this bulk value, as discussed below.

C_{mf} = salt concentration, C, on membrane surface, m, feed side, f, (ppm). In this application, the feed side of the membrane starts with fresh water, ~700ppm. As this water fluxes across the membrane, and salt passes from the permeate to the feed side, this

concentration grows, and can reach 8000ppm, depending on membrane sizing. Because it is at the membrane surface rather than in the bulk flow, C_{mf} is slightly different from the bulk flow concentration, as discussed below.

Unfortunately, the osmotic pressure that applies in Equation A2 is the pressure across the membrane, not the osmotic pressure between the two bulk fluids. This requires some way of knowing the salt concentration at the membrane surfaces. If there were no water flux across the membrane, the salt concentration at the surfaces would be the same as that in the bulk flow. Instead, the buildup of salt at the surface is proportional to the flux of water across it. This buildup is termed 'concentration polarization'. A way to parameterize this issue is to use 'β', which is the ratio of the salt concentration at the surface over that in the bulk flow:

$\beta = C_m/C_{bulk}$, i.e. $\beta_f = C_{mf}/C_f$ and $\beta_p = C_{mp}/C_p$. (A3)

Where β = concentration polarization factor (unitless). β_f = feed side, β_p = permeate side.

C_m = concentration at the membrane surface (ppm). C_{mf} = feed side, C_{mp} = permeate side.

C_f = feed side bulk concentration (ppm). C_p = permeate side bulk concentration.

In a typical reverse osmosis application, there is only one beta value, that of the feed, because only the feed piles up salt as water is pushed from the salty side to the salt-free side. The salt-free side, the permeate, has so little salt in it that there is no need for a β value there. However, in this application, both feed and permeate sides have significant salt concentrations. Hence, both sides have beta parameters to characterize the concentration polarization going on at the two surfaces.

Salt flows across the membrane in proportion to the concentration difference across it; its resistance to flow is chemical and electrical, owing more to its solubility in the membrane material rather than any pressure difference across the membrane. The constant of proportionality is B, where B is defined from:

$J_{salt} = B *(C_{mp} – C_{mf})$ (A4)

Where J_{salt} = salt flux across the membrane per area (ppm*m/s).

B = salt permeability (m/s or GFD)

Note that in normal reverse osmosis operations, $J_{salt} = J*C_p$: the salt flux across the membrane is just the water flux times the salt concentration in the permeate (also, in such cases, $C_{mp} = C_p$, i.e. β_p

=1, as there is no concentration polarization on the permeate side of the membrane). However, in this application that relationship is not assured.

The buildup of salt at the membrane surfaces can be estimated using film theory, refer to Figure A1. Unlike normal RO operations, in this application the water fluxes in one direction as the salt fluxes in the other direction. On the feed side (i.e. freshwater side), freshwater convects salt toward the membrane as diffusion pushes it the other direction. On balance, the two sum up to the salt flux across the membrane (J_{salt}). That is:

Figure A1: Concentration Polarization

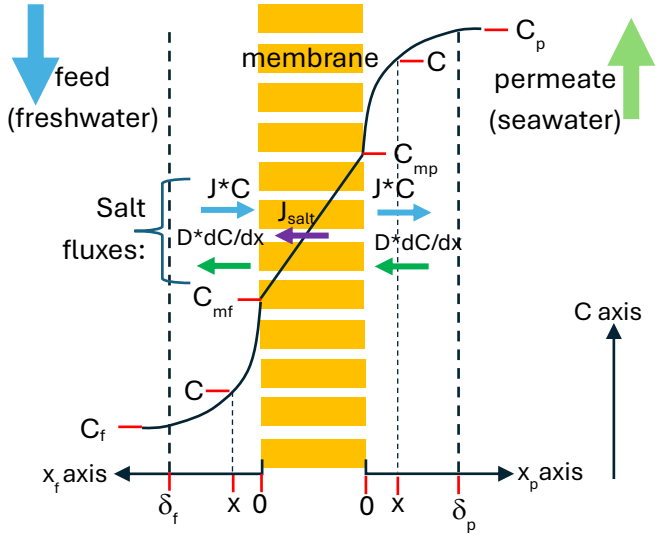

$$J_{salt} = -D*dC/dx - J*C \qquad (A5)$$

Where D = diffusivity of salt in water (m^2/s). D in mass transfer is analogous to the thermal conductivity (k) in heat transfer.

dC/dx = concentration gradient normal to the membrane surface(ppm/m)

J = water flux toward the membrane (m/s).

C = salt concentration at location x from the membrane (ppm)

If x=0 at the membrane and δ_f at the feed-side boundary layer, then integration from $0<x<\delta_f$ yields:

$$(J_{salt} + J*C_{mf}) / (J_{salt} + J*C_f) = \exp(J/k_f) \qquad (A6)$$

Where $k_f = D/\delta_f$ = the mass transfer coefficient, which is analogous to the convection coefficient (h) in heat transfer.

The same procedure done on the permeate side of the membrane yields:

$$(J_{salt} + J*C_p) / (J_{salt} + J*C_{mp}) = \exp(J/k_p), \text{ where } k_p = D/\delta_p \qquad (A7)$$

k and β are both ways of expressing concentration polarization at a surface: to a close approximation, $\beta_f \sim \exp(J/k_f)$ and $\beta_p \sim 1/\exp(J/k_p)$. Therefore, finding k is the path to finding β.

In heat transfer through tubes, experimental nondimensional relationships have been developed relating the Nusselt Number to the Reynolds Number and the Prandtl Number. The same relationships can be used for mass transfer in tubes, by substituting the Sherwood Number in place

of the Nusselt Number and the Schmidt Number in place of the Prandtl Number. The Sherwood Number includes the mass transfer coefficient, k, in its formulation, so the use of these relationships from fluid mechanics, heat and mass transfer studies is the path to understanding concentration polarization (i.e. β) in this application.

For the permeate side of this application, assuming turbulence (i.e. Re>3000), the relationship used (Equation 8.62 in [6]):

$$Sh_p = (f/8)*(Re_p - 1000)*Sc / [1 + 12.7*(f/8)^{0.5} *(Sc^{0.66} - 1)] \quad (A8)$$

Where Sh_p = Sherwood No = k_p*d_{hp}/D, Re_p = Reynolds No = v_p*d_{hp}/ν, Sc = Schmidt No = ν/D

f = fanning friction factor = $\xi(R_{ep}$, wall roughness)

d_{hp} = hydraulic diameter of the tube (m). For spiral wound membranes this is twice the gap between adjacent leaves of the spiral wound module.

v_p = velocity of the permeate (m/s)

ν = kinematic viscosity of water (m^2/s)

Formally, Equation A8 is valid for a nonporous surface. An example would be the surface of a lake past which dry air is blowing. The presence, in this case, of a porous surface lifting the boundary layer requires that the result from equation 8 be adjusted downward. The method for doing this is discussed in Appendix B.

Evaluating the feed side was more complicated, because the water flow is significantly impacted by the feed spacer filling it's 33mil gap (a gap less than 2% of the gap on the permeate side). The feed side is kept geometrically similar to that of standard spiral wound RO modules to allow usage of Sherwood Number correlations specifically developed from test data on such modules. Four such correlations were investigated. Although they all provided very different Sherwood Numbers for the same geometry, flow, and fluid conditions (Sh = f(Re,Sc)), each was appropriate for the membrane and pressure regime individually examined in their derivation. A method was worked out to choose which correlation to use in this application and is discussed in Appendix B. Once that selection method was developed, the selected Sherwood correlation could be used on the feed side of the membrane, providing a final equation for solution of the system.

Evaluating the ocean RO exchanger starts with knowing the membrane permeabilities, A and B. Although these two permeabilities are generally considered to be constants of the membrane, both are significantly affected by temperature. The generally understood relationship is that these permeabilities drop about 3% for each 1 C drop in water temperature (equation 2.65 in [7]. FilmTec uses a slightly different calculation [16] but it has a similar result). At the depth of the power plant the temperature is about 16C instead of the 25C that membranes are usually tested at. This was accounted for in calculations, as was the effect of water temperature on other properties of water such as density, viscosity, and diffusivity.

Also known are the incoming feed and permeate side conditions: the flow rates (gpm) and salt concentrations (ppm) of the incoming streams on both sides of the membrane. Whether evaluated as a single item or broken up into multiple consecutive stages in a chain, at each stage the salt concentration can be calculated based on the permeations from the previous stages, so salt concentrations (C_f and C_p) can be estimated through mass and salt balances.

Flow conditions on the feed and permeate sides of the membrane are encapsulated through calculation of the Reynolds Number (Re_f, Re_p) from the flow rates and geometries, which also allows calculation of the fanning friction factor (f). The physical properties of water (D, ν, Sc) were all adjusted for its temperature. For saltwater, the constant iR= 0.2504 Pa/ppm-K, as discussed previously.

To solve the ocean RO exchanger then requires finding six unknowns simultaneously: J, Jsalt, β_f, β_p, k_f, and k_p. The six equations available are given below:

$$J = A *[P – iR*T*(\beta_p*C_p – \beta_f*C_f)] \quad (A9)$$

$$J_{salt} = B *(\beta_p*C_p – \beta_f*C_f) \quad (A10)$$

$$(J_{salt} + J* \beta_f*C_f) / (J_{salt} + J*C_f) = \exp (J/k_f) \quad (A11)$$

$$(J_{salt} + J*C_p) / (J_{salt} + J* \beta_p*C_p) = \exp (J/k_p) \quad (A12)$$

$$k_p*d_{hp}/D = Sh_p = (f/8)*(Re_p – 1000)*Sc / [1 +12.7*(f/8)^{0.5} *(Sc^{0.66} – 1)] \quad (A13)$$

$$k_f*d_{hf}/D = Sh_f = f(Re_f, Sc) \text{ from Sherwood correlation for spiral wound RO module} \quad (A14)$$

Equation A9 comes from combining equations A1, A2, and A3. Equation A10 comes from combining equations A3 and A4. Equation A11 comes from combining equations A3 and A6, and equation A12 from combining equations A3 and A7. Equation A13 comes from restating equation A8 in terms of k_p. Equation A14 is taken from previously developed Sherwood Number correlations for the feed sides of spiral wound RO modules.

In practice, solution started by estimating values for β_f and β_p. This allows the solution of J and J_{salt} in equations A9 and A10. Separate evaluation of k_f and k_p via equations A13 and A14 allows β_f and β_p to be reevaluated in equations A11 and A12, completing the circle until it converges. Separately, mass and salt balances were maintained to ensure C_f and C_p were kept consistent with the water and salt fluxes being calculated.

In spreadsheet form, two models were maintained, a single-node model and a ten-node model. The single-node model was assisted by a five-node mini-model for mass and salt balancing calculations.

In the ten-node model, the permeate and feed flows were in parallel flow, to simplify the calculation. In actual usage, a counterflow arrangement is probably ideal. The permeate is seawater which is flowing at such a high volume that the error is negligible, as it is not greatly affected by its passage through the RO exchanger.

The single- and ten-node models converged on similar answers, which was a check on the overall reliability of the solution approach. For example, in calculating output power the difference was less than 1%.

Appendix B: Accounting for Concentration Polarization

The significance of Concentration Polarization

Equation A1 defines the membrane water permeability, A. The inverse of this is the membrane water resistivity, ρ:

$$\rho = (P - OsmP) / J \quad = 1/A \qquad (B1)$$

The total system resistivity to water flux through the system is more than ρ, however. Due to the added resistivity of the two 'concentration polarization' layers that build up on the membrane surfaces in operation, it can be quite a bit more. Defining the 'total system resistivity' as:

$$\rho_{tot} = (P - OsmP_{bulk}) / J \quad = 1/A_{tot} \qquad (B2)$$

Where the 'Bulk Osmotic Pressure' (using equation A2 as a guide) is defined as:

$$OsmP_{bulk} = iRT * (C_p - C_f) \qquad (B3)$$

$OsmP_{bulk}$ is the Osmotic Pressure set up by the user, who defines the salt contents of the feed and permeate streams. OsmP is the Osmotic Pressure across the membrane, which would equal $OsmP_{bulk}$ if there were no concentration polarization. OsmP acts across the membrane resistivity, while $OsmP_{bulk}$ acts across all three resistivities. Considering the definition of OsmP in equation A2, the resistivities of the two 'concentration polarization' layers can be determined as:

$$\rho_f = iRT * C_f * (\beta_f - 1) / J \quad = 1/A_f \qquad (B4)$$

$$\rho_p = iRT * C_p * (1 - \beta_p) / J \quad = 1/A_p \qquad (B5)$$

So that:

$$\rho_{tot} = \rho + \rho_f + \rho_p \quad \text{or, equivalently, } 1/A_{tot} = 1/A + 1/A_f + 1/A_p \qquad (B6)$$

Improving the permeability of the membrane makes for little improvement overall, if concentration polarization in one or both surfaces defines the overall resistance to permeate flux. As an example, using the Ocean RO Power Plant spreadsheet shown in Table 1, with a slow permeate flow velocity (5 cm/s), the four resistivities in equation B6 are: 2.18 = 0.23 + 0.03 + 1.92 (i.e. $\rho_{tot} = \rho + \rho_f + \rho_p$, where resistivity is in units of bar/LMH, where 1 bar = 14.5 psi, and LMH = L/m^2-hr). With a faster permeate flow velocity (25 cm/s), the four resistivities become: 0.6 = 0.23 + 0.03 + 0.34. Without acting to reduce the permeate-side resistivity (due to concentration

Figure B1: Area & ρ_p versus v_p

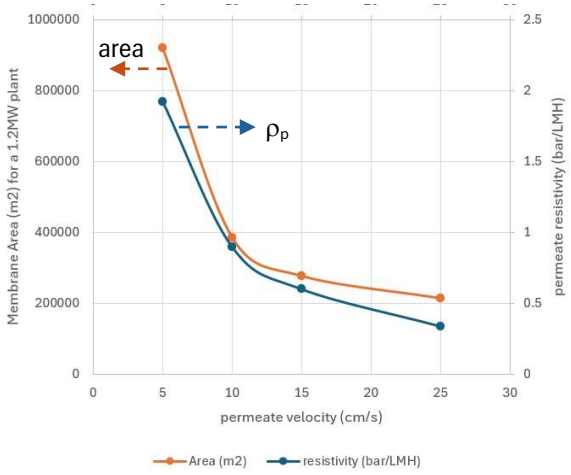

polarization), the actual membrane resistivity makes little difference. The 25 cm/s permeate flow velocity, in producing the same amount of power as the 5 cm/s flow velocity, requires just 25% as much membrane area. Figure B1 graphs this effect of permeate flow velocity on permeate resistivity (ρ_p) and on the required membrane area to produce about 1.2 MW of power. The 25 cm/s case is the one shown in Table 1.

Therefore, given its significance, it is important to properly estimate concentration polarization on both surfaces as part of the Ocean RO power plants design process.

Feed Side Concentration Polarization

Feed side concentration polarization can be estimated from previously published Sherwood Number correlations, assuming similar geometric and fluid flow parameters are used in this novel application [8-11]. Mostly this means retaining a feed side spacer like those used in traditional RO spiral wound modules, which have feed spacer thicknesses of 20 to 40 mil (0.5 to 1 mm).

The Sherwood Number should strictly be a function of geometry and fluid flow parameters (Sh = f(Re, Sc). Unfortunately, that was not found to be true in this case. The reason is put down to the porosity of the membrane, which allows the fluid and its properties to 'leak' past the enclosure wall in a manner not easily captured by correlations that assume a nonporous wall. Four correlations were examined for possible use in this application. Given the same Reynolds Number and Schmidt Number, and hydraulic diameter, they all gave significantly different Sherwood Numbers, as shown in Table B1.

Table B1: Sherwood Numbers calculated from five different correlations for the same Reynolds Numbers (Geometry and Schmidt Number also the same)

Re	Qui&Davies[9]	Table 3 [7]	Schock&Miquel[11]	Chen&Qin[10]	Srivathsan[8]
100	5	9	22	22	80
200	6	11	41	41	129
300	7	12	58	60	169
400	8	14	75	78	205

Notes: 1. Schock&Miquel define hydraulic diameter and cross-flow area differently from the other correlations. Most researchers assume the hydraulic diameter is twice the leaf gap, as it would be for a channel composed of two parallel infinite walls. Due to the presence of the feed spacer, it is more complicated than that, and Schock&Miquel accounted for that difference in their correlation. Similarly, the cross-flow area, which in most correlations is the leaf gap times the width, is in Schock&Miquel reduced by the spacer filling the gap. This Table uses a correlation from Schock&Miquel that is corrected for these differences to be more equitably compared to the other correlations.
2. Chen&Qin experimented with glucose as solute. This Table uses their correlation with salt as solute to be equivalent to the others (the solute affects the Diffusivity and Schmidt Number).

As examples of these Sherwood Number correlations:

the Chen&Qin correlation [10] is $Sh = 0.031 * Re^{0.9243} * Sc^{0.3495}$ (B7)

and the Qui&Davies correlation [9] is $Sh = 1.015 * Re^{0.335} * Sc^{0.34} * (dh/L)^{0.33}$ (B8)

Except for the correlation listed in Table 3 in [7] (which was for laminar channel flow), each paper was attended by sufficient experimental data to back up the correlation's derivation. Therefore, each correlation appears to be correct for its experimental situation.

Since the flow, fluid, and geometry parameters are the same in Table B1, the difference between these correlations is expected to be related to their differing permeate flux rates (J), which is related to the permeability of the membrane and the pressure regime and salt concentrations examined in each study. Specifically, a high permeate flux rate should reduce the boundary layer on the feed side, which would increase the Sherwood number above what a nonporous surface assumption would calculate. Higher J means higher Sh.

The Sherwood Number is sought to help quantify concentration polarization. To help determine which of the above correlations to use in the Osmotic Engine, their experimental data was examined to help calculate a 'Sherwood Value', similar to the Sherwood Number, from parameters affecting the permeate flux, J. In a normal RO application, from film theory (and so derived similarly to the derivation of equation A6 in Appendix A):

$$\exp(J/k_f) = (\beta_f * C_f - C_p)/(C_f - C_p) \quad \text{(B9)}$$

From the definition of the salt permeability 'B' and knowing that in a normal RO application, $J_{salt} = J*C_p$ (i.e. the salt fluxing through the membrane is just the water fluxing through it times its salt content):

$$J_{salt} = J*C_p = B*(\beta_f * C_f - C_p) \quad \text{(B10)}$$

Combining these two equations, isolating k_f and multiplying by d_h/D defines the 'Sherwood Value':

$$Sv = (d_h/D)*\{ J / \ln[J*(1-R_o)/(B*R_o)] \quad \text{(B11)}$$

Where R_o = salt rejection = $1 - (C_p/C_f)$. Note that (C_p/C_f) is typically referred to as 'salt passage' (SP) so $R_o = 1 - SP$, and $Sv = (d_h/D)*\{ J / \ln[J*SP/(B*(1-SP)]$

Sv = 'Sherwood Value'. This ideally equals the Sherwood Number (Sh) if all experimental parameters are measured perfectly. Sv will be estimated in this application to help determine which Sherwood correlation in Table B1 to use to ultimately calculate Sh.

Equation A1 relates the permeate flux, J, to the membranes water permeability (A), the pressure (P) and the Osmotic Pressure (OsmP, which is strongly affected by concentration polarization: β_f). Hence, in equation B11, the 'Sherwood Value' is purely a function of the membrane itself (A, B, SP), pressure, salt content, and concentration polarization. Although it ideally equals the Sherwood Number, Sh, the Sherwood Number is calculated with no reference to any of those membrane-specific parameters:

$$Sv = \xi(A, B, P, OsmP, \beta_f, SP) \sim Sh = \xi(Re, Sc, \text{geometry such as } d_h \text{ and } L) \quad \text{(B12)}$$

Sv is mostly a function of the permeate flux, J, which in an experiment is measured. In the four correlations examined and listed in Table B1, sufficient experimental data was available to determine the Sv number for which each Sh correlation applied. Figure B1 graphs the four correlations Sh output versus their Sv number.

Figure B1: Four Sh correlations, sorted by Sv number

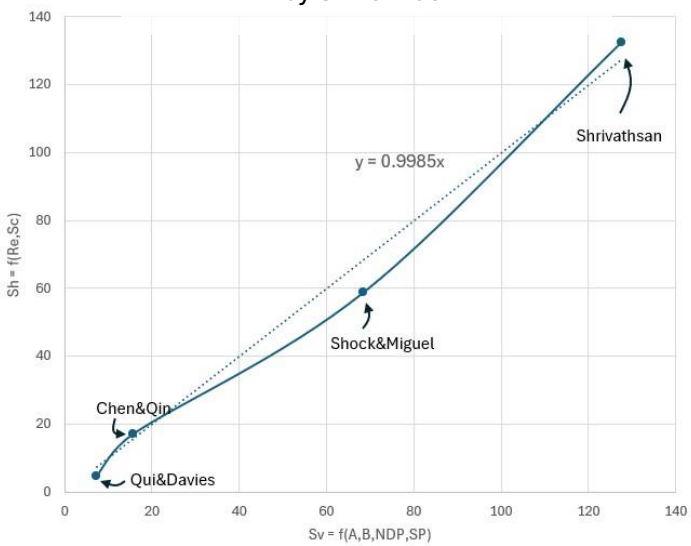

As expected, each experiment calculates Sherwood numbers approximately equal to their Sherwood values, for the given conditions. For application to this Ocean Osmotic Engine, however, the Sherwood Value was first estimated from the membrane parameters 'A' and 'B', the Net Driving Pressure (P and OsmP), and the estimated amount of concentration polarization (β_f). Once the Sherwood Value was estimated, a Sherwood Number correlation was chosen from among the four available. For almost all conditions, so far, the Chen&Qin correlation has been chosen. This is essentially the same as choosing the Schock&Miguel correlation (see Table B1), which is an often-used industry standard. However, near the bottom of the RO exchanger, when the feed-side salt concentrations become higher, which causes more concentration polarization, the Qui&Davies correlation can sometimes be chosen. The Srivathsan correlation was derived for seawater desalination at high pressure: it's permeate flux rates are much higher than are derived in this application, so has not been chosen so far.

Permeate side Concentration Polarization

Unlike the concentration polarization on the feed side, the permeate side has 'dilution polarization': incoming fresh water dilutes seawater near the surface, leading to salt concentrations that are lower at the surface than in the bulk fluid. That is, $\beta_f > 1$, but $\beta_p < 1$. Since the incoming permeate flux, J, is normal to the permeate flow direction, its effect is to lift the boundary layer away from the channel wall: $\delta_{porous} > \delta_{nonporous}$. In equation A6, A7, and A8, the mass transfer coefficient is defined as $k = D/\delta$, and the Sherwood Number is defined as $Sh = k*d_h/D$, where D is salt diffusivity. Combining these two definitions:

$$\delta*Sh = d_h \qquad (B13)$$

Where d_h = hydraulic diameter, which is the same whether the channel wall is porous or nonporous. Hence,

$$Sh_{porous} / Sh_{nonporous} = \delta_{nonporous} / \delta_{porous} \quad \text{(B14)}$$

In equation B7 and B8, the parameter δ is referring to the concentration boundary layer. In turbulent flow, the concentration boundary layer is approximately the same size as the mechanical boundary layer, so changes to the mechanical boundary layer can be assumed to also apply to the concentration boundary layer.

In turbulent flow in channels, according to the 'law of the wall' (equation 8.29 in [12]) the boundary layer is traditionally identified as the outer edge of the viscous sublayer, which is located by:

$$\delta = 5*\nu/u* \quad \text{(B15)}$$

Where ν = kinematic viscosity of water (m^2/s) and u* is the 'friction velocity', defined as:

$$u* = (\tau_w/\rho)^{½} \quad \text{(B16)}$$

where ρ = density (kg/m^3) and τ_w is the wall shear stress, which can be calculated from the pressure drop in the channel (plus geometry), or alternatively from the fanning friction factor and permeate velocity:

$$\tau_w = d_h*\Delta p/(4*L) = (f/4)*(\rho*v_p^2/2) \quad \text{(B17)}$$

d_h = hydraulic diameter of the tube (m, i.e. twice the permeate-side gap)

Δp = pressure drop through the channel (Pa). L = length of the channel (m).

f = fanning friction factor = $\xi(R_{ep}$, wall roughness). ρ = density (kg/m^3).

v_p = velocity of the permeate (m/s)

Water fluxes through the porous channel wall with no component of velocity along its length. This causes the boundary layer to grow. The amount of this growth, at the mid-point of the channel, can be estimated using:

$$\Delta\delta = J * (L/v_p)/2 \quad \text{(B18)}$$

Where (L/v_p) is the residence time of seawater in the permeate channel, in seconds. The average boundary layer in a porous channel is thus:

$$\delta_{porous} = \delta_{nonporous} + \Delta\delta \quad \text{(B19)}$$

With this, and using equation B8, Sh_{porous} can be calculated. It is generally 20% to 30% lower than $Sh_{nonporous}$, which is calculated using equation A8. For the ten-node model, $\Delta\delta$ was adjusted throughout the length of the channel to more appropriately estimate the growth of the boundary layer along that length.

Appendix C: Using commercial RO test data to determine membrane permeabilities A and B

Commercial RO specifications often do not specify the permeabilities A and B outright. When an RO membrane is tested it is part of a spiral wound module, so the results include the module specifications [13]. Two testing parameters often quoted are the 'Recovery' (rec) and the 'salt rejection' (R_o). 'Recovery' refers to the amount of feed saltwater to the module that is 'recovered' as freshwater. i.e. rec = Q_p/Q_f. Salt rejection ($R_o = 1 – [C_p/C_f]$) is referring to the ability of the system to reject salt from the permeate product stream. The 'salt passage' (SP) may be given instead of R_o, where $SP = C_p/C_f = 1\text{-}R_o$.

Isolating the membrane specific permeabilities requires an estimate of how much feed-side concentration polarization, β_f, was occurring during testing (in normal RO usage there is no permeate concentration polarization since the permeate is too low in salt content, i.e. $\beta_p = 1$). To estimate β_f while testing an RO module, a useful industry approximation (equation 2.57 in [7]) is:

$$\beta \sim K_p * \exp(Q_p/Q_b) \quad \text{(C1)}$$

Where $K_p = 0.99$ (based on industry experience), $Q_p = J*\text{Membrane Area (S)}$, and Q_b = average feed flow through the module, i.e. $Q_b = (Q_f + Q_c)/2$, where Q_f and Q_c are the feed flow rate into, and out of, the module. Often instead of Q_c the 'Recovery' (rec) of the module, or system of modules, is given instead. In that case, $Q_c = Q_f*(1\text{-rec})$. In a normal RO setting, equation B9 indicates that, to a close approximation (assuming $C_f >> C_p$): $\beta \sim \exp(J/k)$, hence equation C1 is expressing that Q_b is related to k as Q_p is related to J, namely by the Membrane Area (S).

Once β is estimated, the membrane permeabilities can be estimated directly. Salt permeability can be calculated using equation B10 rearranged:

$$B = J / [\beta*(C_b/C_p) - 1] \quad \text{(C2)}$$

To calculate A, combine the definition of water permeability in equations A1, A2, and A3 (keeping only β_f by setting $\beta_p = 1$), with the salt permeability definition from equation B10:

$$A = J / [P - iRT*C_p*(J/B)] \quad \text{(C3)}$$

Since equation C1 only provides an estimate of β, it is better to choose a Sherwood Number correlation to estimate k, and then derive β from k using equation B9 or the approximation $\beta \sim \exp(J/k)$. To do this, estimate a Sherwood Value (Sv) using the estimate of β and then select a Sherwood Number correlation to use for the more accurate value.

Equation B11 requires B to be known to evaluate Sv. As an alternative, start by inserting the definition $R_o = 1 – (C_p/C_f)$ into equation B9 and rearranging:

$$J/k = \ln\{[(\beta\text{-}1)/R_o] + 1\} \quad \text{(C4)}$$

Since $Sv = (d_h/D)*k = (d_h/D)*J/(J/k)$, then:

$$Sv = (d_h/D)*J/\ln\{[(\beta\text{-}1)/R_o] + 1\} \quad \text{(C5)}$$

So Sv can be estimated given the β estimate from equation C1, and the salt rejection, R_o, or salt passage, SP = 1- R_o. Then a Sherwood Number correlation can be chosen and, given Re and Sc, a more accurate k value calculated, from which a more accurate β value, using equation C4 again, and, finally, B and A, using equations C2 and C3.

Sometimes, membrane testing involved a system of modules rather than just one RO module. In that case, the rejection Ro or salt passage, SP, may be given in terms of the entire system rather than for just one module. The permeabilities can still be estimated. For example, in one case, 14 modules were set up in series [14]. The water permeability (A) was given but the salt permeability (B) had to be derived from the other information given, specifically the overall salt passage. The overall salt passage can be calculated from $SP_{all} = C_{pavg} / C_f$, where $C_{pavg} = \Sigma(C_{pi}*J_i)/\Sigma J_i$. Here, i refers to module i of the 14 modules and C_f is the incoming feed salt concentration to the entire system. Knowing that $SP_i = C_{pi} / C_{bi}$, and that $C_{pi}*J_i = J_{salti} = B*(\beta_i*C_{bi} – C_{pi})$ where C_{bi} is the bulk feed concentration from approximately the middle of module i (and recalling that for normal RO operations there is no concentration polarization on the permeate side of the membrane), then:

$$SP_i = B*\beta_i/(J_i-B) \quad \text{(C6)}$$

Since B is approximately a constant for all modules, it's value can be determined as a function of the overall salt passage (SP_{all}) and the various module specific parameters, C_{bi}, β_i, and J_i:

$$SP_{all}*C_f = \Sigma(C_{bi}*(B*\beta_i/(J_i-B))*J_i)/\Sigma J_i \quad \text{(C7)}$$

As before, isolating the membrane specific permeabilities requires an estimate of how much concentration polarization was occurring during testing, for which equation C1 is useful.